

1 **Continental Scale Assessment of Variation in Floodplain Roughness**
2 **with Vegetation and Flow Characteristics**

3
4 **Gabriel Barinas^{1,2,*}, Stephen P. Good^{1,2}, and Desiree Tullos^{1,2}**

5 ¹Water Resources Graduate Program, Oregon State University

6 ²Department of Biological & Ecological Engineering, Oregon State University

7 * Corresponding author: Gabriel Barinas (barinasg@oregonstate.edu)

8
9 **Key Points:**

- 10 • 4,927 estimates of floodplain roughness were calculated using flow observations and
11 compared to LiDAR vegetation data.
- 12 • Floodplain roughness increases with increasing biomass and inundation depths and
13 decreases with increasing flow velocity.
- 14 • Our model's Manning's n estimates yield lower errors in reach-scale floodplain flow
15 predictions than n based solely on land cover.
- 16

17 **Abstract**

18 Quantifying floodplain flows is critical to multiple river management objectives, yet how
19 vegetation within floodplains dissipates flow energy lacks comprehensive characterization.
20 Utilizing over 3.4 million discharge measurements, in conjunction with aboveground biomass
21 and canopy height measurements from NASA's Global Ecosystem Dynamics Investigation
22 (GEDI), this study characterizes the floodplain roughness coefficient Manning's n and its
23 determinates across the continental United States. Estimated values of n show that flow
24 resistance in floodplains decreases as flow velocity increases but increases with the fraction of
25 vegetation inundated. A new function (RMSE = 0.024, $r^2 = 0.74$) is proposed for predicting n
26 based on GEDI vegetation characteristics and flow velocity, with GEDI derived n values
27 improving predictions of discharge relative to those based only on land cover. This analysis
28 provides evidence of key hydraulic patterns of energy dissipation in floodplains, and integration
29 of the proposed function into flood and habitat models may reduce uncertainty.

30

31 **Plain Language Summary**

32 Quantifying the capacity of floodplains to dissipate energy from flowing water is important in
33 managing rivers, restoring habitats, and reducing flood risks. By integrating overbank flood
34 characteristics measured at USGS gauging stations with vegetation properties of floodplains
35 measured by NASA, this study analyzed how energy dissipation in the floodplain, via a
36 hydraulic roughness coefficient, varies with vegetation biomass and flood depths. Results
37 indicate that floodplain roughness increases with the density of vegetation and decreases with
38 flow velocity. A new mathematical function is presented to estimate floodplain roughness based
39 on remotely sensed vegetation properties for various velocities.

40 **1 Introduction**

41 Floods are one of the most damaging natural disasters affecting society, costing billions
42 of dollars in damages every year (Smith, 2020). Understanding these events is important for the
43 protection of urban and agricultural development, risk management, and ecosystem restoration
44 actions (Bulti & Abebe, 2020). Accordingly, a wide variety of hydraulic models have been
45 developed for prediction and forecasting of river response to flood events and restoration actions,
46 with the vast majority of these model predictions dependent on how a floodplain roughness
47 attenuates flow (Hunter et al., 2007). Manning's equation (Manning, 1891) is the most widely
48 used hydraulic formula relating roughness to discharge and velocities in river channels and
49 floodplains (Yen, 1992). Its application requires knowledge of the geometric characteristics of
50 the channel (area, hydraulic radius, and slope) as well as a key roughness coefficient, n . This
51 empirical coefficient is used to account for energy dissipated due to friction losses, but it is rarely
52 measured directly in the field (R. Ferguson, 2013) due to logistics and safety concerns, and it is
53 difficult to predict for a future land use policy or engineering design. As a result, Manning's n is
54 typically specified from simplified lookup tables (Chow, 1959; Cowan, 1956), and studies have
55 demonstrated that uncertainties in n can lead to large errors in depth and discharge estimates
56 (Durand et al., 2016; Lee & Mays, 1986).

57 Manning's equation in irrigation canals (Manning, 1891) has traditionally attributed
58 energy losses in open channels primarily to vegetation. Lookup tables, such as those by (Chow,
59 1959), include specific n values for different land cover types, indicating the influence of
60 vegetation on Manning's n . While most studies focus on flow resistance of vegetation in the main
61 channel, limited attention has been given to variations in floodplain vegetation resistance during
62 inundation events (R. Ferguson, 2013; Yen, 2002). Prior models (Fathi-Maghadam & Kouwen,

63 1997; Kouwen & Fathi-Moghadam, 2000; Petryk, 1975) of flow resistance for emergent
64 vegetation, highlighted vegetation density as the most important factor contributing to Manning's
65 n , and suggest n varies with the square root of the vegetation inundation fraction and inversely
66 with flow velocity. However, these models were developed spanning limited conditions, e.g.
67 only four individual trees of different types tested in (Kouwen & Fathi-Moghadam, 2000), and
68 remain difficult to parametrize in practice. Furthermore, human modifications to floodplains,
69 including the replacement of vegetation with agricultural fields, roads, and urban development,
70 have altered floodplain roughness. Artificial structures like levees further decrease floodplain
71 extent and disrupt land cover, reducing energy dissipation in the remaining floodplain (Knox et
72 al., 2022). Consequently, the original vegetation classes developed for canals may no longer
73 adequately explain floodplain roughness in overbank areas.

74 The main goal of this study was to characterize roughness in floodplains across the
75 continental US and its relationship with flow and vegetation characteristics. Specially, we
76 examined how floodplain roughness varied with flow velocity, vegetation inundation fraction,
77 and floodplain biomass. Direct estimates of floodplain Manning's n were produced using field
78 measurements collected by the United States Geological Survey (USGS) during overbank flows.
79 Estimated n values were then related to remotely sensed vegetation height and biomass data to
80 quantify their influence on energy dissipation in floodplains. Finally, an empirical function was
81 developed to characterize interactions between floodplain roughness, velocity, and vegetation
82 properties. Additionally, we conducted cross-validation analyses to validate our methodology
83 and compared our results with existing approaches for estimating floodplain roughness.

85 2 Materials and Methods

86 In this study, Manning's equation is applied specifically to the floodplain, separate from
 87 the main river channel. The floodplain discharge is isolated by subtracting the discharge within
 88 the main channel from the total measured discharge (see Supporting Information Figure S1 for a
 89 schematic of the floodplain as defined in this study). Values of Manning's n are then derived by
 90 inverting Manning's equation and solving for the floodplain roughness (see Supporting
 91 Information) during periods of overbank flow (Reclamation, 2001). The necessary parameters
 92 for calculation of n are obtained from field measurements datasets provided by the USGS
 93 (USGS, 2021a). The flood stage height is determined by the National Weather Service (NWS,
 94 2021; Slater et al., 2015), and friction slope estimates are obtained from the National
 95 Hydrography Dataset (NHD) (USGS, 2021b). Estimates of n were constrained to those sites
 96 meeting strict quality control metrics including consistency with current USGS rating curves and
 97 observed channel geometries (Liu, 2011; Vinutha et al., 2018).

$$98 \quad Q = \frac{k}{n} S^{1/2} R^{2/3} A \quad (\text{eq. 1})$$

99 where Q is discharge [$\text{L}^3 \text{t}^{-1}$], S is the friction slope, defining the energy loss along a reach [L L^{-1}],
 100 R the hydraulic radius [L], A is cross-sectional area [L^2], k is a unit conversion factor, and n is
 101 Manning's roughness coefficient.

102 At USGS gauging stations where n values are estimated, vegetation characteristics, such
 103 as aboveground biomass density and vegetation canopy height, are obtained from NASA's
 104 Global Ecosystem Dynamics Investigation (GEDI) (Potapov et al., 2021). GEDI is a LiDAR
 105 system mounted on the International Space Station that provides calibrated values of vegetation
 106 height and biomass globally at a 25m base resolution and gridded final products at 1km

107 resolution (Dubayah et al., 2021, 2022; Milenković et al., 2022) . Previous research suggests that
108 Manning's roughness coefficient is related to vegetation inundation fraction, flow velocity, and
109 vegetation properties (Chow, 1959; Yen, 1992; Rob Ferguson, 2013). A semi-empirical function
110 of n is formulated, based on prior models, that incorporates GEDI-derived vegetation properties.
111 The function parameters are determined by fitting a linearized equation to values of Manning's
112 roughness coefficient, flow velocity, and aboveground biomass at USGS sites. For a detailed
113 explanation of the methodology please refer to the Extended Methodology section S1 in the
114 supplementary information document.

115 To assess the performance of our newly developed function, we conducted a cross-
116 validation analysis, which involved the application of Manning's equation to compute floodplain
117 flow during observed overbank events. This process utilized the same measurements acquired by
118 the USGS, along with Manning's n values estimated through a five-fold cross-validation
119 approach (detailed in the Supplementary Information). Importantly, the Manning's n values used
120 for fitting our function were distinct from those employed to validate discharge calculations at
121 these sites.

122 To comprehensively evaluate our method, we compared the results not only against the
123 directly measured discharge but also against discharges calculated using estimated roughness
124 coefficients from other studies. These alternative approaches include the Geospatial Stream Flow
125 Model (GeoSFM) proposed by (Asante et al., 2008), which parameterizes Manning's n values for
126 different land cover classes for use in a distributed hydrologic model. This model integrates
127 geospatial and time-series data in near-real time, generating daily forcing evapotranspiration and
128 precipitation data from various remote sensing and ground-based sources. GeoSFM employs
129 widely available terrain, soil, and land cover datasets for initial model setup and parameter

130 estimation, making it adaptable for data-scarce environments. The model performs geospatial
131 preprocessing and postprocessing tasks and hydrologic modeling within an ArcView GIS
132 environment, offering seamless integration of GIS routines and time series processing. It
133 identifies and maps wide-area streamflow anomalies, disseminating daily results, including
134 streamflow and soil water maps, through various channels (Internet map servers, flood hazard
135 bulletins, and more).

136 Additionally, Kalyanapu et al., (2009) determined Manning's n values by land cover class
137 in a hydrologic modeling study focused on understanding the effects of land cover use on runoff
138 and peak discharge. This research assesses the sensitivity of hydrologic models to Manning's n
139 changes, a parameter crucial for representing surface roughness. Large watershed models often
140 rely on land use/land cover datasets to assign Manning's n values based on land use or cover
141 classes. While this approach is convenient, it introduces potential errors. Kalyanapu's study
142 compared Manning's n values derived from manual inspection of aerial photos to those estimated
143 using the National Land Cover Dataset (Homer et al., 2012). The results revealed significant
144 differences in the magnitude and spatial distribution of Manning's n values, particularly at
145 subcatchment levels. These differences, while not significantly altering runoff responses at the
146 watershed outlet for large-scale models, became pronounced with increasing Manning's n
147 deviation.

148 To ensure a fair and consistent comparison, we standardized our analysis using the
149 International Geosphere-Biosphere Programme (IGBP) land cover classification (Loveland et al.,
150 1999). Within this framework, we calculated the median velocity and median flow depth for each
151 land cover class and subsequently derived the Manning's n value using our model. This approach
152 allowed us to assess the performance of our function in relation to established methodologies and

153 gain valuable insights into its efficacy in estimating floodplain roughness. We use medians
154 instead of raw values to address the potential bias introduced by the inherent relationship
155 between velocity and roughness, allowing for a fairer comparison against methodologies that do
156 not consider velocity during the selection process.

157

158 **3 Results**

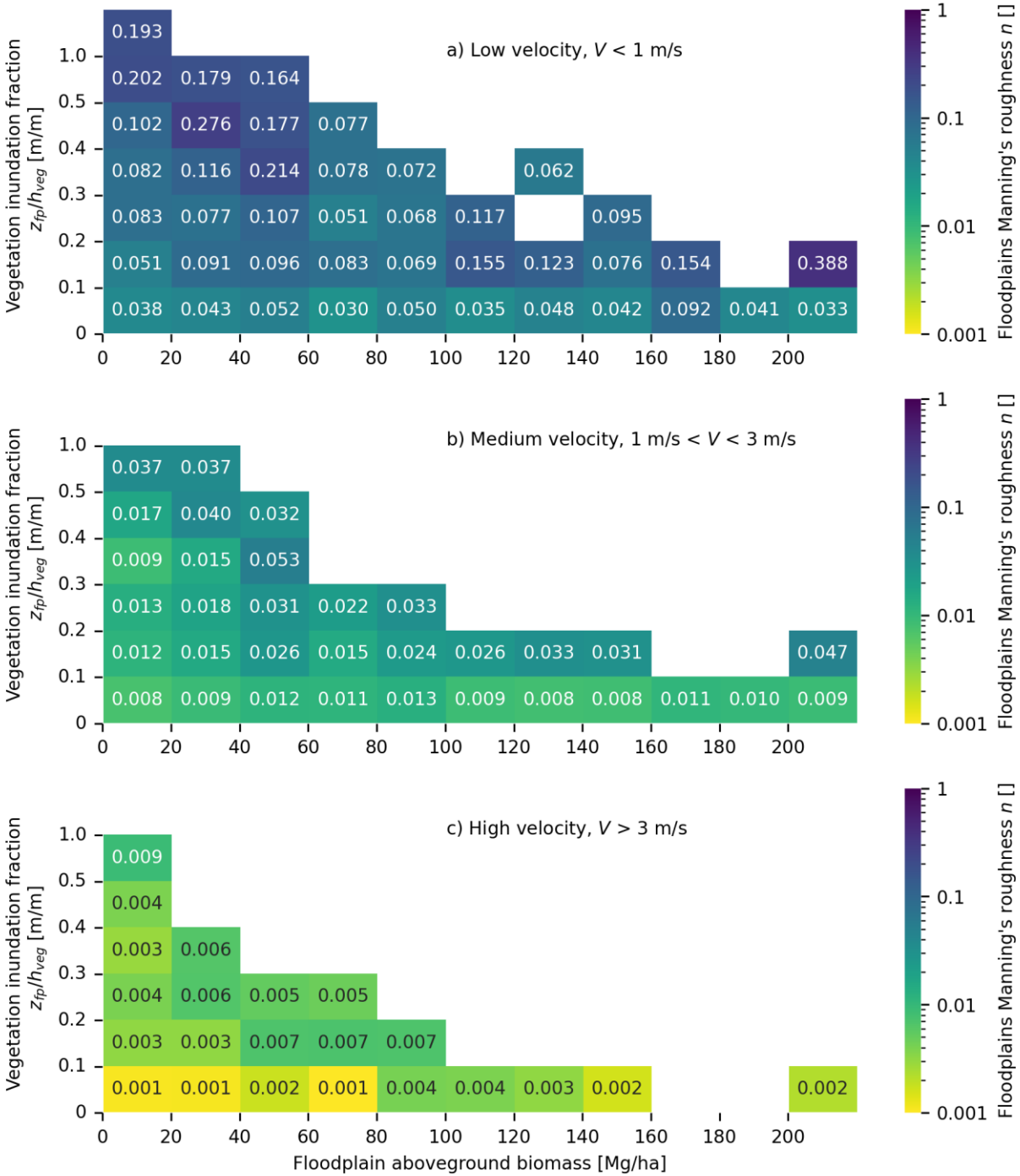
159 After data processing and quality control, a total of 4,927 estimates of floodplain
160 Manning's n were calculated successfully at 804 sites, based on the analysis of 3,379,166 total
161 measurements obtained from 31,142 unique gauge sites (Barinas et al., 2023). Included with this
162 dataset of generated n values (see dataset in Supporting Information) are all the necessary
163 variables measured by the USGS that were used when inverting Manning's equation to solve for
164 n : measured discharge (Q), width (w), depth (z) obtained from USGS field measurements, and
165 friction slope (S) from the NHD datasets. Intermediate variables are also included in this dataset:
166 discharge, velocity, width, and depth, for both the main channel (Q_{mc} , V_{mc} , w_{mc} , z_{mc}) and the
167 floodplain (Q_{fp} , V_{fp} , w_{fp} , z_{fp}). Complementary information included in the dataset are the USGS
168 site ID, date of measurement, coordinates, and number of values of n calculated at that site.

169 Examining all floodplain roughness estimates over the continental United States, the
170 national median of the estimated floodplain Manning's n values was 0.021, with a 5th and 95th
171 percentile of 0.001 and 0.326, respectively. On average, a mean of 18 values of n were obtained
172 per site, with an average of 155 values per state. Site-averaged n values revealed consistent
173 spatial patterns across the continental United States (see Supporting Information Figure S2).
174 These patterns are influenced by factors like vegetation biomass and velocities (Figure 1).

175 Vegetation biomass was shown to drive variability in floodplain roughness, with values
176 of n for different vegetation classes and heights compiled in Table S1 in the Supplementary
177 Information). Areas dominated by Grasses, Shrubs, and Woodland, the most common vegetation
178 classification in the GEDI dataset, tended to have a median Manning's n value of 0.017 for a
179 median biomass on the analyzed sites of 18 Mg/Ha. Deciduous Broadleaf Trees, the second most
180 common class, exhibited slightly higher roughness with a median Manning's n value of 0.025,
181 having a median biomass of 77 Mg/Ha. Evergreen Broadleaf and Evergreen Needleleaf, despite
182 having similar biomass densities (95 Mg/Ha and 106 Mg/Ha, respectively) contributed to
183 different roughness values, with median Manning's n values of 0.030 and 0.010, respectively.
184 Due to a limited number of samples, there were not enough observations to draw conclusions
185 about the impact of Deciduous Needleleaf Trees on floodplain roughness (see Supplementary
186 Information Table 1).

187 Even at a broad scale with the relatively low-resolution, remotely-sensed vegetation
188 (GEDI) datasets used in this project, clear patterns were found between the floodplain Manning's
189 n values and features (i.e. biomass, submergence) expected to predict n values at various velocity
190 ranges (Figure 1). The values of n were inversely related to flow velocity and positively related
191 to vegetation inundation fraction. Velocities were lowest at locations where Manning's n was
192 highest. Within three velocity ranges, Manning's n varied with inundation fraction and
193 vegetation biomass. Median Manning's n values ranged from 0.001-0.009 for the highest
194 velocities ($V > 3$ m/s), whereas median n values ranged between 0.008 and 0.053 for mid-range
195 velocity flows (1-3m/s). Under these mid to high velocities ($V > 1$ m), Manning's n increased
196 consistently with the inundation fraction and inconsistently with vegetative biomass. For low

197 velocity flows ($<1\text{m/s}$), n ranged from 0.030 up to 0.388 and increases in roughness were
 198 associated inconsistently with both inundation fraction and vegetative biomass.

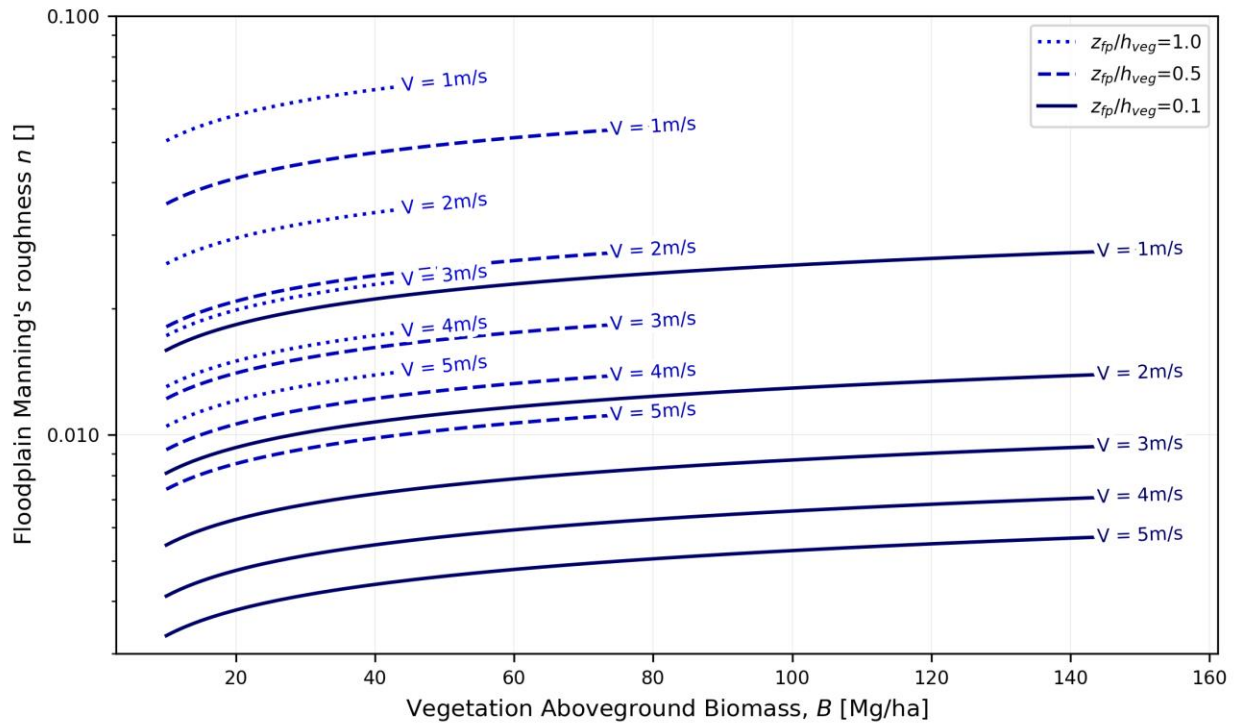


200 **Figure 1.** Median floodplain Manning's n values for different levels of floodplain aboveground
 201 biomass and vegetation inundation fraction. Numerical values within each box represent the
 202 median n value for the corresponding range of vegetation inundation fraction and aboveground
 203 biomass and results shown only when at least five values are available.

204 Based on calculated n values, observed flow velocities (V) and depths within the
 205 floodplain (z_{fp}), as well as GEDI estimated vegetation height (h_{veg}) and biomass (B), an
 206 empirical function relating Manning's n (See Extended Methodology S1) provided a reasonable
 207 fit to observed data ($r^2 = 0.74$):

$$208 \quad n = 0.0321 \frac{B^{0.20}}{V^{0.99}} \left(\frac{z_{fp}}{h_{veg}} \right)^{0.5} \quad (\text{eq. 2})$$

209 This function, visualized across observed conditions in Figure 2, predicted n with a root
 210 mean squared error (RMSE) of 0.024 (see scripts in Supporting Information). It further
 211 illustrated how Manning's n varies with flow and vegetation properties, with an inverse
 212 proportionality between Manning's n and flow velocity. A difference in roughness of nearly one
 213 order of magnitude was found between low velocities ($<1\text{m/s}$) and very high velocities (up to
 214 5m/s) (Figure 2). Within specific velocity ranges, the values of n are notably influenced by
 215 vegetation inundation fraction, with greater roughness associated with higher levels of inundated
 216 vegetation. Furthermore, the data and function demonstrated that biomass tended to increase
 217 roughness more at low biomass levels (visually inspecting tangent lines revealed the inflection
 218 point to be approximately 30 Mg/Ha), whereas its influence decreased at higher biomass levels.
 219 This could explain why the function had less predictive power with biomass at higher levels of
 220 vegetation inundation fractions; High inundation fractions were not frequently observed at high
 221 biomass levels.



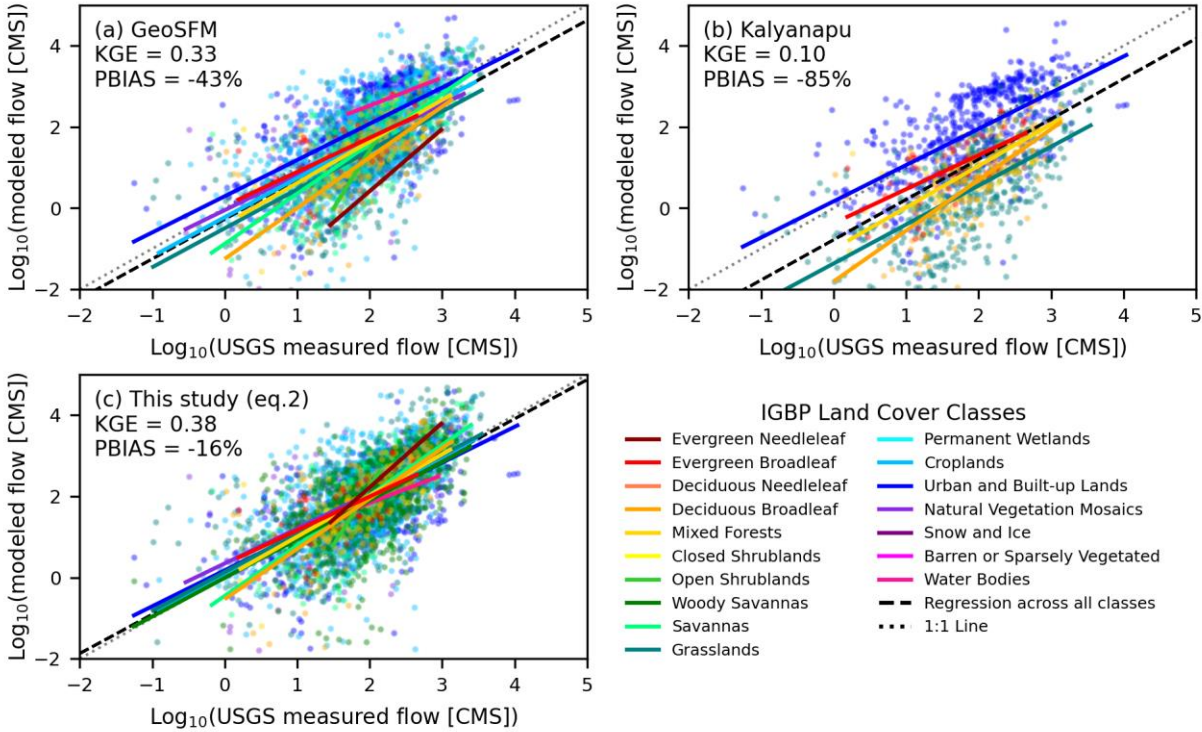
222

223 **Figure 2** – Manning's n modelled as a function of aboveground biomass, B , and flow velocity,
 224 V , modeled for different levels of vegetation inundation fraction (z_{fp}/h_{veg}). Lines extend up to
 225 biomass levels of 50, 80 and 150 Mg/ha for fractions of inundation of 1.0, 0.5 and 0.1,
 226 respectively based on the total number of values within each range as depicted in Figure 1.

227

228 The cross-validation analysis conducted in this study reveals the performance of the
 229 proposed function in estimating USGS measured flows (Figure 3). Our findings indicate that this
 230 function offers higher accuracy and less dispersion, as evidenced by a Kling-Gupta efficiency
 231 (KGE) of 0.38 and a percent bias (PBIAS) of -16%. In comparison, alternative methods for
 232 determining roughness coefficients yielded less accurate results, with KGE values of 0.33 and
 233 0.10, and PBIAS values of -43% and -85% for GeoSFM and Kalyanapu et al. (2009),
 respectively.

234



235

236 **Figure 3** - Measured vs. estimated discharge based on three approaches to estimating floodplain

237 roughness: (a) the Geospatial Stream Flow Model (GeoSFM), (b) Kalyanapu et al's study (2009)

238 on land-use effects on model outputs, and (c) from the function developed in this study (eq. 2).

239 These were calculated with median velocities and median flow depths per land cover class.

240 Kling-Gupta efficiency (KGE) and percent bias (PBIAS) are reported across all vegetation

241 classes.

242

243 4 Discussion

244 Floodplains serve critical functions for society through dissipation of flood energy,

245 among other functions, but understanding of floodplain hydraulics contains large uncertainties

246 due in part to limited field observations of floodplain roughness. This study produced new

247 estimates of floodplain roughness coefficients that span the range of the continental United
248 States. The average estimates of floodplain Manning's n calculated in this study were similar to n
249 values modeled from field measurements of vegetation features (Kouwen & Fathi-Moghadam,
250 2000) and the values in Chow's look-up table (Chow, 1959). Chow identified the range of
251 average n values for floodplains as being from 0.040 (in cleared land with stumps) up to 0.150
252 (for dense willows). In comparison, the average n estimates in this dataset were 0.060 for low
253 canopy height and low levels of biomass, and 0.090 for high canopy height and biomass.

254 Kouwen and Fathi-Moghadam's (2000) study also presented mean values of n for four tree types
255 that range between 0.100 for high velocity flows (2 m/s) and 0.200 for very low velocity flows
256 (0.1 m/s) for submerged conditions ($z_{pf}/h_{veg}=1$), dropping down to a range of 0.030 to 0.070 for
257 low inundation ($z_{pf}/h_{veg}=0.1$). A similar pattern was observed in mean values of floodplain n in
258 this study (Figure 2), ranging from 0.030 for low inundation and comparable velocity ($V = 1-3$
259 m/s), up to an average of 0.250 for low velocity ($V < 1$ m/s) and high inundation fraction. The
260 approach presented here has the advantage of applying global, remotely sensed biomass datasets,
261 compared with Kouwen and Fathi-Moghadam's vegetation index, which requires local
262 measurements of frequency, mass, and height of the trees.

263 Field observations revealed that Manning's n in floodplains was generally lower at higher
264 velocities than at lower velocities. Even though in practice Manning's n is often assumed to be a
265 constant value solely determined based on the characteristics of the surface, in reality it has been
266 demonstrated that n varies with discharge (Box et al., 2021; Chow, 1959; R. Ferguson, 2013). In
267 most river channels, Manning's n decreases as discharge and stage increase due to lower
268 roughness along the banks and the submergence of bed forms with increasing flow depths
269 (USGS, 2012). This phenomenon is also consistent with the long history of roughness in pipe

270 flow studies (Rouse, 1943). Like river channels, where previous research has shown that flow
271 and velocity tend to have an inverse relationship with flow resistance, our calculations
272 demonstrate a similar pattern in floodplains. This alignment with existing research suggests that
273 flow and velocity in both river channels and floodplains exhibit an inverse relationship with flow
274 resistance (Chow, 1959; R. Ferguson, 2013). Mechanistically, the inverse relationship could be a
275 result of higher roughness reducing velocities, or the bending of flexible vegetation that reduces
276 roughness at higher velocities. Datasets presented herein are inadequate for determining the
277 source of the relationship.

278 This work demonstrated that GEDI's vegetation characteristics can be used to estimate
279 floodplain roughness. Vegetation inundation fraction was an important predictor of Manning's n ,
280 as demonstrated in other settings (Nepf, 2012). In addition, this national Manning's n database
281 reflects how floodplain roughness increases with aboveground biomass, though relative
282 inundation demonstrated a stronger influence on roughness than biomass. This makes sense
283 given that a key factor influencing Manning's n is the total vegetation cross section obstructing
284 flow, not just the height of the canopy (Chow, 1959). Furthermore, previous studies have found
285 that the density of vegetation in channels was a dominant parameter for Mannings's n in
286 emergent conditions (Fathi-Maghadam & Kouwen, 1997) and the analysis here demonstrated
287 that this finding translated to the floodplain as well. Since GEDI measures these vegetation
288 properties globally, estimations of floodplain roughness can be extended worldwide with this
289 method, with some caveats discussed below.

290 As previously outlined in the methodology section, our assessment involved a cross-
291 validation analysis of the function defined in Equation 2. This process included the application of
292 Manning's equation (eq. 1) to calculate floodplain flow during observed overbank events, using

293 measurements from the US Geological Survey (USGS) and Manning's n coefficients estimated
294 by our function. We also compared our findings with discharge estimates obtained from previous
295 studies by Asante et al. (2008) and Kalyanapu et al. (2009), offering valuable insights into the
296 robustness of our approach.

297 Our cross-validation analysis reveals notable advantages of the proposed function, which
298 is rooted in US Geological Survey (USGS) gage data. This function demonstrated superior
299 performance with a Kling-Gupta efficiency (KGE) of 0.38 and a percent bias (PBIAS) of -16%
300 in estimating USGS measured flows. In comparison, alternative methods for determining
301 roughness coefficients, such as GeoSFM (KGE = 0.33, PBIAS = -43%) and Kalyanapu's
302 approach (KGE = 0.10, PBIAS = -85%), yielded less accurate results. Importantly, the other
303 methods consistently underestimated flow rates across various land cover types when relying on
304 constant roughness coefficients. This artifact is due to land cover –roughness coefficient
305 classifications being defined based on steady and uniform flow conditions in channels (Chow,
306 1959) and not accounting for variation of resistance with changing flow, especially during flood
307 events with higher flow rates. This is evident in the fact that the hydrologic models analyzed in
308 these works utilized hydrographs, which involve unsteady flow characterized by changing flow
309 over time. As a consequence, the roughness coefficient becomes variable in reality but not in the
310 models. By incorporating a vegetation- and submergence-dependent Manning's n coefficient, the
311 proposed function captured varying hydraulic conditions, leading to improved flow estimates
312 when compared to methods that rely on a roughness coefficient that is independent of hydraulic
313 conditions. Supporting this interpretation, both the GeoSFM and Kalyanapu et al. (2009)
314 methods demonstrated relatively accurate estimates for short vegetation classes such as urban

315 areas, built-up lands, and croplands, although they still lacked the precision displayed by our
316 function in this study.

317 The Manning's n dataset and the function proposed in Eq. 2 have the potential to improve
318 the performance of large-scale models such as the National Water Model (NWM). Many
319 attempts are currently being made to reduce uncertainty in nationwide models (Johnson et al.,
320 2019; Rojas et al., 2020), but have been focused on improving its performance by updating the
321 geometry and roughness parameters of the main channel, without extending improvements to the
322 floodplain (Heldmyer et al., 2022). Integrating the results from this work on floodplain
323 roughness at USGS gauge locations into the NWM could be a logical next step.

324 Our study introduces a novel approach to enhance the NWM, especially during flood
325 events, by incorporating dynamic floodplain roughness values. These values account for
326 variations in flow velocity and vegetation properties, essential factors that are traditionally
327 treated as constants in large-scale models. This integration offers the potential for more accurate
328 flood predictions, improved flood risk assessments, and enhanced river management strategies.
329 It's important to acknowledge the possibility of adjustments to other key parameters, such as
330 channel roughness. While our study doesn't prescribe a specific approach for these adjustments,
331 it opens an intriguing avenue for future research and collaboration.

332 The study datasets were subject to some limitations, including those inherent to the USGS
333 monitoring network (Kiang et al., 2013; Tu et al., 2023), as discussed in the SI. Gaging
334 limitations may narrow the generalizability of the results to LULCs (Land Use Land Cover) and
335 geographic regions included in this gaging network. Further, assumptions about the geometry of
336 a river's cross-section were made that could be inconsistent in some channels, such as where the
337 local slope is too high or width too narrow to maintain that a hydraulic radius that is

338 approximately equal to the hydraulic depth. Furthermore, the vegetation phenology is a snapshot
339 in time, though it has been established that considerable differences exist in vegetation
340 characteristics between seasons that can impact flow (Bond et al., 2020). To provide high-quality
341 biomass and height estimates, the GEDI averages measurements. The resulting derived products
342 do not represent a specific time of year, in contrast with USGS field measurements that were
343 made on a specific date. Finally, vegetation data were sampled from GEDI's 1 km² gridded
344 product for the area around each USGS gauge site, which leads to questions regarding what area
345 influences Manning's roughness. Energy dissipation occurs via multiple processes during a flood
346 (R. Ferguson, 2013), but the area of influence that has a direct effect on flow is poorly
347 understood and is worthy of further study. The assumption made for these calculations is that the
348 1 km² average for the vegetation characteristics taken from GEDI measurements is representative
349 of the actual area influencing energy dissipation during a flood. This assumption may not be
350 valid at sites where there is a large variation in land cover within a 1 km² grid.

351

352 **5 Conclusions**

353 Floodplain roughness is a critical aspect of managing floodplains, and its societal
354 relevance will rise with rising floodwaters under climate change, expanding floodplain
355 development, aging flood infrastructure, and rising emphasis on floodplain reconnection for
356 nature-based flood infrastructure and ecological restoration. While Manning's n is typically
357 assumed to be a constant value in floodplain analysis and engineering applications, this study
358 demonstrated that accurate estimation of current and modified floodplain roughness should rely
359 on vegetation submergence and velocities, with biomass playing a smaller role.

360 The dataset of floodplain Manning's n generated in this work, and its correlation with
361 flow and vegetation characteristics, further supported prior findings that flow resistance during a
362 flood increases with submergence depth and biomass, and that resistance is inversely related to
363 flow velocity. This work utilized a unique coupling of existing datasets, considering tall
364 vegetation biomes, and demonstrated how flow and vegetation properties influence roughness
365 across a wide range of regions and climates in the continental United States, rather than limited
366 to a specific site or sites. Results should be generalizable across scales and landscapes that align
367 with the input datasets and should support the management and restoration community in
368 establishing sustainable floodplains.

369 **Acknowledgments**

370 We would like to acknowledge the support of the Fulbright Program and Oregon State
371 University through the Graduate Fellowship program. This project has been partially funded by
372 the NASA grant 80NSSC21K0198 award to Stephen Good. We would also like to thank Cara
373 Walter and Harrison Lee Kutz for their support with the processing and retrieval of NHD and
374 GEDI data.

375 **Open Research**

376 The scripts to reproduce the dataset, figures and tables in this study are openly available
377 at Barinas et al. (2023) under a Creative Commons Attribution License format (free registration
378 required).

379 **6 References**

- 380 Asante, K. O., Artan, G. A., Pervez, S., Bandaragoda, C., & Verdin, J. P. (2008). Technical
381 manual for the geospatial stream flow model (GeoSFM). *World Wide Web*, 605, 594–
382 6151.
- 383 Barinas, G., Good, S., & Tullos, D. (2023). Dataset and Supporting Information for Barinas et.
384 al. Floodplain Roughness Study [Data set]. CUAHSI HydroShare. Retrieved from
385 <https://doi.org/10.4211/hs.8c5b71cf3a7449b0b94c447a3e87e63f>
- 386 Bond, S., Kirkby, M. J., Johnston, J., Crowle, A., & Holden, J. (2020). Seasonal vegetation and
387 management influence overland flow velocity and roughness in upland grasslands.
388 *Hydrological Processes*, 34(18), 3777–3791. <https://doi.org/10.1002/hyp.13842>
- 389 Box, W., Järvelä, J., & Västilä, K. (2021). Flow resistance of floodplain vegetation mixtures for
390 modelling river flows. *Journal of Hydrology*, 601, 126593.
391 <https://doi.org/10.1016/j.jhydrol.2021.126593>
- 392 Bulti, D. T., & Abebe, B. G. (2020). A review of flood modeling methods for urban pluvial flood
393 application. *Modeling Earth Systems and Environment*, 6(3), 1293–1302.
394 <https://doi.org/10.1007/s40808-020-00803-z>
- 395 Chow, V. T. (1959). Chow, V. T. (1959). Open-channel hydraulics. McGraw-Hill, New York -
396 Google Search. Retrieved August 28, 2022, from
- 397 Cowan, W. L. (1956). Estimating hydraulic roughness coefficients. *Agricultural Engineering*,
398 37(7), 473–475.
- 399 Dubayah, R. O., Luthcke, S. B., Sabaka, T. J., Nicholas, J. B., Paux, S., & Hofton, M. A.
400 (2021). GEDI L3 Gridded Land Surface Metrics, Version 2. *ORNL DAAC*.
401 <https://doi.org/10.3334/ORNLDAAC/1952>

- 402 Dubayah, R. O., Armston, J., Healey, S. P., Yang, Z., Patterson, P. L., Saarela, S., et al. (2022).
403 GEDI L4B Gridded Aboveground Biomass Density, Version 2. *ORNL DAAC*.
404 <https://doi.org/10.3334/ORNLDAAC/2017>
- 405 Durand, M., Gleason, C. J., Garambois, P. A., Bjerklie, D., Smith, L. C., Roux, H., et al. (2016).
406 An intercomparison of remote sensing river discharge estimation algorithms from
407 measurements of river height, width, and slope: SWOT DISCHARGE ALGORITHM
408 INTERCOMPARISON. *Water Resources Research*, 52(6), 4527–4549.
409 <https://doi.org/10.1002/2015WR018434>
- 410 Fathi-Maghadam, M., & Kouwen, N. (1997). Nonrigid, Nonsubmerged, Vegetative Roughness
411 on Floodplains. *Journal of Hydraulic Engineering*, 123(1), 51–57.
412 [https://doi.org/10.1061/\(ASCE\)0733-9429\(1997\)123:1\(51\)](https://doi.org/10.1061/(ASCE)0733-9429(1997)123:1(51))
- 413 Ferguson, R. (2013). 9.5 Reach-Scale Flow Resistance. In *Treatise on Geomorphology* (pp. 50–
414 68). Elsevier. <https://doi.org/10.1016/B978-0-12-374739-6.00230-X>
- 415 Ferguson, Rob. (2013). 9.5 Reach-Scale Flow Resistance. In *Treatise on Geomorphology* (pp.
416 50–68). Elsevier. <https://doi.org/10.1016/B978-0-12-374739-6.00230-X>
- 417 Heldmyer, A., Livneh, B., McCreight, J., Read, L., Kasprzyk, J., & Minear, T. (2022).
418 Evaluation of a new observationally based channel parameterization for the National
419 Water Model. *Hydrology and Earth System Sciences*, 26(23), 6121–6136.
420 <https://doi.org/10.5194/hess-26-6121-2022>
- 421 Homer, C. H., Fry, J. A., & Barnes, C. A. (2012). The national land cover database. *US*
422 *Geological Survey Fact Sheet*, 3020(4), 1–4.

- 423 Hunter, N. M., Bates, P. D., Horritt, M. S., & Wilson, M. D. (2007). Simple spatially-distributed
424 models for predicting flood inundation: A review. *Geomorphology*, *90*(3), 208–225.
425 <https://doi.org/10.1016/j.geomorph.2006.10.021>
- 426 Johnson, J. M., Munasinghe, D., Eyelade, D., & Cohen, S. (2019). An integrated evaluation of
427 the National Water Model (NWM)–Height Above Nearest Drainage (HAND) flood
428 mapping methodology. *Natural Hazards and Earth System Sciences*, *19*(11), 2405–2420.
429 <https://doi.org/10.5194/nhess-19-2405-2019>
- 430 Kalyanapu, A., Burian, S., & Mcpherson, T. (2009). Effect of land use-based surface roughness
431 on hydrologic model output. *Journal of Spatial Hydrology*, *9*, 51–71.
- 432 Kiang, J. E., Stewart, D. W., Archfield, S. A., Osborne, E. B., & Eng, K. (2013). *A national*
433 *streamflow network gap analysis* (USGS Numbered Series No. 2013–5013). *A national*
434 *streamflow network gap analysis* (Vol. 2013–5013). Reston, VA: U.S. Geological
435 Survey. <https://doi.org/10.3133/sir20135013>
- 436 Knox, R. L., Morrison, R. R., & Wohl, E. E. (2022). A river ran through it: Floodplains as
437 America’s newest relict landform. *Science Advances*, *8*(25), eabo1082.
438 <https://doi.org/10.1126/sciadv.abo1082>
- 439 Kouwen, N., & Fathi-Moghadam, M. (2000). Friction Factors for Coniferous Trees along Rivers.
440 *Journal of Hydraulic Engineering*, *126*(10), 732–740.
441 [https://doi.org/10.1061/\(ASCE\)0733-9429\(2000\)126:10\(732\)](https://doi.org/10.1061/(ASCE)0733-9429(2000)126:10(732))
- 442 Lee, H.-L., & Mays, L. W. (1986). Hydraulic Uncertainties in Flood Levee Capacity. *Journal of*
443 *Hydraulic Engineering*, *112*(10), 928–934. [https://doi.org/10.1061/\(ASCE\)0733-](https://doi.org/10.1061/(ASCE)0733-9429(1986)112:10(928))
444 [9429\(1986\)112:10\(928\)](https://doi.org/10.1061/(ASCE)0733-9429(1986)112:10(928))

- 445 Liu, X. (2011). Accuracy Assessment of Lidar Elevation Data Using Survey Marks. *Survey*
446 *Review*, 43(319), 80–93. <https://doi.org/10.1179/003962611X12894696204704>
- 447 Loveland, T. R., Zhu, Z., Ohlen, D. O., Brown, J. F., Reed, B. C., & Yang, L. (1999). An
448 analysis of the IGBP global land-cover characterization process. *Photogrammetric*
449 *Engineering and Remote Sensing*, 65, 1021–1032.
- 450 Manning, R. E. (1891). On the flow of water in open channels and pipes.
- 451 Milenković, M., Reiche, J., Armston, J., Neuenschwander, A., De Keersmaecker, W., Herold,
452 M., & Verbesselt, J. (2022). Assessing Amazon rainforest regrowth with GEDI and
453 ICESat-2 data. *Science of Remote Sensing*, 5, 100051.
454 <https://doi.org/10.1016/j.srs.2022.100051>
- 455 Nepf, H. M. (2012). Flow and Transport in Regions with Aquatic Vegetation. *Annual Review of*
456 *Fluid Mechanics*, 44(1), 123–142. <https://doi.org/10.1146/annurev-fluid-120710-101048>
- 457 NWS. (2021). USGS WaterWatch - Streamflow conditions. Retrieved November 3, 2022, from
458 <https://waterwatch.usgs.gov/>
- 459 Petryk. (1975). Analysis of flow through vegetation.
- 460 Potapov, P., Li, X., Hernandez-Serna, A., Tyukavina, A., Hansen, M. C., Kommareddy, A., et al.
461 (2021). Mapping global forest canopy height through integration of GEDI and Landsat
462 data. *Remote Sensing of Environment*, 253, 112165.
463 <https://doi.org/10.1016/j.rse.2020.112165>
- 464 Reclamation, U. S. B. of. (2001). *Water measurement manual*. The Bureau. Retrieved from
465 [https://books.google.com/books?hl=es&lr=&id=7PdRAAAAMAAJ&oi=fnd&pg=PA11](https://books.google.com/books?hl=es&lr=&id=7PdRAAAAMAAJ&oi=fnd&pg=PA11&dq=water+measurements+manual+usbr&ots=ajRs6q1ds-&sig=atpXC2u8__bFWTy9ndNikoeB7a8)
466 [&dq=water+measurements+manual+usbr&ots=ajRs6q1ds-](https://books.google.com/books?hl=es&lr=&id=7PdRAAAAMAAJ&oi=fnd&pg=PA11&dq=water+measurements+manual+usbr&ots=ajRs6q1ds-&sig=atpXC2u8__bFWTy9ndNikoeB7a8)
467 [&sig=atpXC2u8__bFWTy9ndNikoeB7a8](https://books.google.com/books?hl=es&lr=&id=7PdRAAAAMAAJ&oi=fnd&pg=PA11&dq=water+measurements+manual+usbr&ots=ajRs6q1ds-&sig=atpXC2u8__bFWTy9ndNikoeB7a8)

- 468 Rojas, M., Quintero, F., & Krajewski, W. F. (2020). Performance of the National Water Model
469 in Iowa Using Independent Observations. *JAWRA Journal of the American Water*
470 *Resources Association*, 56(4), 568–585. <https://doi.org/10.1111/1752-1688.12820>
- 471 Rouse, H. (1943). Evaluation of Boundary Roughness. *Proceedings Second Hydraulic*
472 *Conference, University of Iowa Bulletin 27*.
- 473 Slater, L. J., Singer, M. B., & Kirchner, J. W. (2015). Hydrologic versus geomorphic drivers of
474 trends in flood hazard. *Geophysical Research Letters*, 42(2), 370–376.
475 <https://doi.org/10.1002/2014GL062482>
- 476 Smith, A. B. (2020). U.S. Billion-dollar Weather and Climate Disasters, 1980 - present (NCEI
477 Accession 0209268) [Data set]. NOAA National Centers for Environmental Information.
478 <https://doi.org/10.25921/STKW-7W73>
- 479 Tu, T., Comte, L., & Ruhi, A. (2023). The color of environmental noise in river networks.
480 *Nature Communications*, 14(1), 1728. <https://doi.org/10.1038/s41467-023-37062-2>
- 481 USGS. (2012). USGS Data Series 668: Manning’s Roughness Coefficients for Illinois Streams.
482 Retrieved September 29, 2022, from
483 https://pubs.usgs.gov/ds/668/pdf/DataSeries_668_2.pdf
- 484 USGS. (2021a). Measurements - Surface Water for USA: Streamflow Measurements. Retrieved
485 August 25, 2022, from <https://waterdata.usgs.gov/nwis/measurements>
- 486 USGS. (2021b). National Hydrography Dataset | U.S. Geological Survey. Retrieved August 25,
487 2022, from <https://www.usgs.gov/national-hydrography/national-hydrography-dataset>
- 488 Vinutha, H. P., Poornima, B., & Sagar, B. M. (2018). Detection of Outliers Using Interquartile
489 Range Technique from Intrusion Dataset. In S. C. Satapathy, J. M. R. S. Tavares, V.

490 Bhateja, & J. R. Mohanty (Eds.), *Information and Decision Sciences* (pp. 511–518).

491 Singapore: Springer. https://doi.org/10.1007/978-981-10-7563-6_53

492 Yen, B. C. (1992). *Channel Flow Resistance: Centennial of Manning's Formula*. Water

493 Resources Publication.

494 Yen, B. C. (2002). Open Channel Flow Resistance. *Journal of Hydraulic Engineering*, *128*(1),

495 20–39. [https://doi.org/10.1061/\(ASCE\)0733-9429\(2002\)128:1\(20\)](https://doi.org/10.1061/(ASCE)0733-9429(2002)128:1(20))

496